

A General 3D Geometry-Based Stochastic Model for Industrial IoT Environments

Yang Liu^{1,2,3,4}, Cheng-xiang Wang^{1,4,*}, Rong Dai³, Xin Guo³, Yu Yu⁵

¹National Mobile Communications Research Laboratory, School Information of Science and Engineering, Southeast University, Nanjing 210096, China.

²State Key Laboratory of Millimeter Waves, Southeast University, Nanjing 210096, China

³Ministerial Key Laboratory of Advanced Control for Light Industry Processes, Jiangnan University, Wuxi 214122, China

⁴Purple Mountain Laboratories, Nanjing 211111, China

⁵School of Information and Communication Engineering, Nanjing Institute of Technology, Nanjing 211167, China

*Corresponding author: Cheng-xiang Wang

Email: ly71354@163.com, chxwang@seu.edu.cn, daisy dluu@163.com, 984464113@qq.com, yuyu@njit.edu.cn

Abstract—Industrial Internet of things (IoT) environment is one of the typical scenarios in the beyond fifth generation (B5G) networks. In this paper, a general three dimensional (3D) geometry-based stochastic model (GBSM) is proposed for the industrial IoT environments. Typical channel parameters, such as the power, delay, azimuth angle of arrival (AAOA), azimuth angle of departure (AAOD), elevation angle of arrival (EAOA), elevation angle of departure (EAOD) are combined to model the channel impulse response (CIR). The spatial consistency of the parameter is achieved by the sum of sinusoids (SOS) method. The spatial non-stationarity is modeled by describing the birth and death of the clusters under the industrial environments. To support the broadband channel, the CIR is modeled at each bin of the whole spectrum and the frequency correlation of the parameters is taken into account. Extensive simulated and measured results validate the credibility of the proposed model.

I. INTRODUCTION

The beyond fifth generation (B5G) wireless communication systems have been widely studied recently. Industrial Internet of things (IoT) environment is one of the typical scenarios in the B5G networks. In the industrial IoT environment, the cooperation and automatic control can be achieved by the multi-source information interactions between the machines. Thus, the industrial IoT channel should support the ultra-reliable and low latency communication (uRLLC). Analysis and modeling of the channel characteristics are very important to construct an uRLLC network under the industrial IoT environment.

The channel characteristics under the industrial environments have been intensively studied since 1987 [1]-[3]. The modeled and measured results under the industrial environments have been reported in the past decades. Generally, they could be categorized into five distinctive types. The first type was the large scale fading model. Influences of the distances between the transmitter (Tx) and the receiver (Rx), the central frequencies, and the obstacles on the path loss had been measured and modeled [4]-[6]. The second type was to model the number of multipaths. The typical distributions, such as Poisson, Beta and Gaussian, were utilized to model

the number of the multipaths [2],[4]. The third type was about the correlations of the channel parameters, such as the root mean square (RMS) delay spread, the shadowing factor (SF) and the Tx-Rx distance [5],[7]. The empirical correlation models of the above parameters were established for various scenarios. The fourth type was about the amplitude fading [8]-[11]. The distributions, i.e., Rician, Nakagami, segment-Nakagami and mixed Gamma-Lognormal were used to model the amplitude fadings under the line-of-sight (LOS) and the non-LOS (NLOS) environments. The fifth type was about the channel impulse response (CIR) [12]-[14]. Based on the Saleh-Valenzuela (SV) model, the CIR was simulated and analyzed.

Basically, the above models mainly focused on the single-input-single-output (SISO) channels. However, SISO technology can not realize the uRLLC system. To construct the uRLLC system for the industrial IoT environment, massive multiple-input- multiple-output (MIMO) combined with the millimeter wave (mmwave) technology should be utilized. Massive MIMO technology can support multiple users to share the same transmitted resources and mmwave can provide the sufficient spectrum for the communication systems. Thus, the characteristics of the massive MIMO channel at the mmwave band for the industrial environment should be considered. As the number of antennas increases, the massive MIMO channel exhibits the spatial non-stationarity [15]. The geometry-based stochastic model (GBSM) in [16] described the spatial non-stationarity of the massive MIMO channel, but the spatial consistency of the channel parameters was not considered. Although the 3GPP and QuaDRiGa models supported the spatial consistency of the parameters [17]-[18], the spatial non-stationarity was not taken into account. A spatial non-stationary and spatially consistent channel model will be more important for the industrial IoT scenarios. Motivated by this reason, a general three dimensional (3D) GBSM for the industrial IoT environments is proposed. The main contributions of this paper are

- A CIR model combined of several typical channel param-

eters, such as the power, delay, azimuth angle of arrival (AAOA), azimuth angle of departure (AAOD), elevation angle of arrival (EAOA), and elevation angle of departure (EAOD), is proposed for the industrial environments. The spatial consistency of the channel is modeled by the sum of sinusoids (SOS) method.

- The spatial non-stationarity of the massive MIMO channel is modeled by describing the birth and death of the clusters under the industrial environments.
- This proposed model is suitable for the broadband channel under the industrial IoT environment. The CIR model is established at each bin of the whole bandwidth and the frequency correlations of the parameters are considered.

II. A GENERAL 3D GBSM FOR INDUSTRIAL IoT ENVIRONMENTS

The schematic diagram of the proposed GBSM is shown in the Fig. 1. Base station (BS) is a large array composed of N_B antennas, and user side (US) is composed of N_U distributed antennas. This paper considers the uplink where US is the Tx and BS is the Rx. To illustrate clearly, only the l^{th} ($l=1, 2, \dots, N_{qp}$) NLOS path is shown in this figure, where N_{qp} is the total number of NLOS paths between the p^{th} transmitted antenna A_p^R and the q^{th} received antenna A_q^R . $\mathbf{A}_p^R(t)$ and $\mathbf{A}_q^R(t)$ are the position vectors of A_p^R and A_q^R , respectively. This model adopts the two-bounce propagation mechanism. The l^{th} path is represented by a pair of clusters, i.e., the first-bounce cluster C_l^A and the last-bounce cluster C_l^Z . \mathbf{C}_l^A and \mathbf{C}_l^Z are the position vectors of C_l^A and C_l^Z , respectively. $\mathbf{D}_q^{lm}(\mathbf{D}_p^{lm})$ is defined as the distance vector from A_q^R (A_p^R) to the rays within C_l^Z (C_l^A). \mathbf{D}_{qp}^L is the distance vector of the LOS path from A_p^R to A_q^R . Also, $\phi_{qplm}^{AAOA}(\phi_{qplm}^{EAOA})$ is defined as the azimuth (elevation) angle from the m^{th} ray of the cluster C_l^Z to A_q^R and $\phi_{qplm}^{AAOD}(\phi_{qplm}^{EAOD})$ is defined as the azimuth (elevation) angle from A_p^R to the m^{th} ray of the cluster C_l^A , respectively. ϕ_{qpL}^{AAOD} , ϕ_{qpL}^{AAOA} , ϕ_{qpL}^{EAOD} , ϕ_{qpL}^{EAOA} are the AAoD, AAoA, EAoD, EAoA of the LOS path from A_p^R to A_q^R , respectively. The movements of the Tx, Rx, C_l^A , C_l^Z are denoted by the speeds v^X , where $X = \{T, R, A, Z\}$. The parameters are summarized in Table I.

A. Proposed 3D GBSM

A 3D GBSM for the industrial environments is proposed. On the basis of 3GPP standardized channel model [17], the spatial non-stationary characteristics and the spatial consistency are considered in the proposed model. Furthermore, this proposed model is suitable for the broadband channel.

Let $h_{qpf}(\tau, t)$ represents the CIR between A_p^R and A_q^R at the f^{th} frequency bin. The CIR can be expressed as a sum of the LOS and NLOS components

$$h_{qpf}(\tau, t) = \sqrt{\frac{K(t)}{K(t)+1}} h_{qpf}^L(\tau) \delta(\tau - \tau_{qp}^L(t)) + \sqrt{\frac{1}{K(t)+1}} \sum_{l=1}^{N_{qp}(t)} \sum_{m=1}^{M_l} h_{qplm}(t) \delta(\tau - \tau_{qp}^{lm}(t)) \quad (1)$$

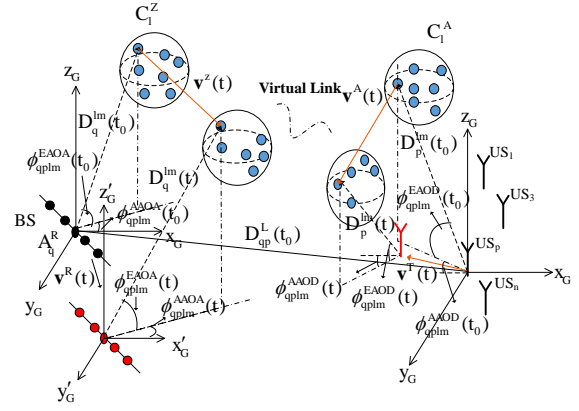


Fig. 1. The schematic diagram of the proposed GBSM model

where $p = 1, 2, \dots, M_T$, $q = 1, 2, \dots, M_R$, and $f = 1, 2, \dots, N_F$. $K(t)$ is the Rician factor.

The LOS components can be expressed as (2) at the top of the next page, where \cdot^T denotes the transpose operation. $\tau_{qp}^L(t)$ is the delay of the LOS path at time t . The functions F_{pf}^V (F_{pf}^H) and F_{qf}^V (F_{qf}^H) are the antenna patterns of A_p^R (A_q^R) for the vertical and horizontal polarizations, respectively. θ_L^V and θ_L^H are the initial phases with uniform distributions over $(0, 2\pi]$. $\mathbf{r}_p^L(t)$ and $\mathbf{r}_q^L(t)$ are the unit vectors in the direction of departure and arrival angle of the LOS path between A_p^R and A_q^R , respectively. λ_f denotes the wavelength of the f^{th} bin. $\nu_{qp}^L(t)$ represents the time variant Doppler shift of the LOS components and can be expressed as

$$\nu_{qp}^L(t) = \frac{\mathbf{r}_q^L(t) \cdot (\mathbf{v}^R(t) - \mathbf{v}^T(t))}{\lambda_f} \quad (3)$$

The NLOS components can be expressed as (4) at the top of the next page, where $P_{qp}^{lm}(t)$, $\tau_{qp}^{lm}(t)$ are the power and delay of the m^{th} ray within the l^{th} cluster. M_l is the total number of rays within the l^{th} cluster. $\mathbf{r}_p^{lm}(t)$ ($\mathbf{r}_q^{lm}(t)$) is the unit vector in the direction of departure (arrival) angle of the m^{th} ray within the l^{th} cluster. The time variant Doppler shift of the NLOS components can be calculated as

$$\nu_{qp}^{lm}(t) = \frac{\mathbf{r}_p^{lm}(t)(\mathbf{v}^T(t) - \mathbf{v}^A(t)) + \mathbf{r}_q^{lm}(t)(\mathbf{v}^R(t) - \mathbf{v}^Z(t))}{\lambda_f} \quad (5)$$

For the broadband channel, the bandwidth B_c is divided into N_F bins. The range of f^{th} bin is $[f_c - \frac{B_c}{2} + (f-1)\frac{B_c}{N_F}, f_c - \frac{B_c}{2} + f\frac{B_c}{N_F}]$. The CIR at each bin can be modeled as same as above. Then the transfer function at each bin can be achieved by Fourier transform. Finally, the transfer functions over the whole bandwidth can be obtained by adding the transfer functions of all bins.

$$H_{qpf}(\xi, t) = \int_{-\infty}^{+\infty} h_{qpf}(\tau, t) e^{-j2\pi\xi\tau} d\tau \quad (6)$$

$$H_{qp}(\xi, t) = \sum_{f=1}^{N_F} H_{qpf}(\xi, t) \quad (7)$$

TABLE I
SUMMARY OF KEY PARAMETER DEFINITION

Symbol	Definition
A_p^T/A_q^R	The p^{th}/q^{th} Tx/Rx antenna
$\mathbf{A}_p^T/\mathbf{A}_q^R$	position vectors of A_p^T/A_q^R
C_l^A/C_l^Z	first/last-bounce cluster of the l^{th} path
$\mathbf{C}_l^A/\mathbf{C}_l^Z$	the position vectors of C_l^A/C_l^Z
$\phi_{qpL}^{AAOD}/\phi_{qpL}^{EAOD}$	AAOD/EAOD of the LOS path from A_p^T to A_q^R
$\phi_{qpL}^{AAOA}/\phi_{qpL}^{EAOA}$	AAOA/EAOA of the LOS path from A_p^T to A_q^R
$\phi_{qplm}^{AAOD}/\phi_{qplm}^{EAOD}$	AAOD(EAOD) of the m^{th} ray impinging in C_l^A from A_p^T
$\phi_{qplm}^{AAOA}/\phi_{qplm}^{EAOA}$	AAOA(EAOA) of the m^{th} ray impinging in A_q^R from C_l^Z
$\mathbf{D}_q^{lm}/\mathbf{D}_p^{lm}$	distance vector between $A_q^R(t)/A_p^T(t)$ and the m^{th} ray within C_l^Z/C_l^A

$$h_{qp}^L(t) = \begin{bmatrix} F_{qf}^V(\phi_{qpL}^{AAOA}, \phi_{qpL}^{EAOA}) \\ F_{qf}^H(\phi_{qpL}^{AAOA}, \phi_{qpL}^{EAOA}) \end{bmatrix}^T \begin{bmatrix} e^{j\theta_L^{VV}} & 0 \\ 0 & -e^{j\theta_L^{HH}} \end{bmatrix} \begin{bmatrix} F_{pf}^V(\phi_{qpL}^{AAOD}, \phi_{qpL}^{EAOD}) \\ F_{pf}^H(\phi_{qpL}^{AAOD}, \phi_{qpL}^{EAOD}) \end{bmatrix} \quad (2)$$

$$\times \sqrt{\sum_{l=1}^{N_{qp}(t)} \sum_{m=1}^{M_l(t)} P_{qp}^{lm}(t)} \times e^{-j2\pi(\frac{|\mathbf{D}_{qp}^L(t)| - \mathbf{r}_q^L(t) \cdot \mathbf{A}_q^R(t) - \mathbf{r}_p^L(t) \cdot \mathbf{A}_p^T(t)}{\lambda_f} + \nu_{qp}^L(t))}$$

$$h_{qp}^{lm}(t) = \begin{bmatrix} F_{qf}^V(\phi_{qplm}^{AAOA}(t), \phi_{qplm}^{EAOA}(t)) \\ F_{qf}^H(\phi_{qplm}^{AAOA}(t), \phi_{qplm}^{EAOA}(t)) \end{bmatrix}^T \begin{bmatrix} e^{j\Phi_{lm}^{VV}} & \frac{e^{j\Phi_{lm}^{VH}}}{\sqrt{k_{lm}(t)}} \\ \frac{e^{j\Phi_{lm}^{HV}}}{\sqrt{k_{lm}(t)}} & e^{j\Phi_{lm}^{HH}} \end{bmatrix} \begin{bmatrix} F_{pf}^V(\phi_{qplm}^{AAOD}(t), \phi_{qplm}^{EAOD}(t)) \\ F_{pf}^H(\phi_{qplm}^{AAOD}(t), \phi_{qplm}^{EAOD}(t)) \end{bmatrix} \quad (4)$$

$$\times \sqrt{P_{qp}^{lm}(t)} \times e^{j2\pi(\frac{\mathbf{r}_q^{lm}(t) \cdot \mathbf{A}_q^R(t) + \mathbf{r}_p^{lm}(t) \cdot \mathbf{A}_p^T(t)}{\lambda_f} + \nu_{qp}^{lm}(t))}$$

The CIR can be determined by the Fourier transform

$$h_{qp}(\tau, t) = \frac{1}{2\pi} \int_{-\infty}^{+\infty} H_{qp}(\xi, t) e^{j2\pi\xi\tau} d\xi \quad (8)$$

B. Spatially consistent parameters

When initializing the angles and delays, the SOS method in the QuaDRiGa channel model is utilized to ensure the spatial consistency of the small scale parameters [18]. The steps are illustrated as following.

First, the azimuth and elevation angles are generated according to the initial positions of Tx and Rx. For example, the initial AAOD from A_p^T to C_l^Z can be calculated as

$$\phi_{qpl}^{AAOD}(t_0) = \frac{\pi}{2} \operatorname{erfc} \left(\frac{X_l^\phi(\mathbf{A}_p^T(t_0)) + X_l^\phi(\mathbf{A}_q^R(t_0))}{2} \right) - \frac{\pi}{2} \quad (9)$$

where X_l^ϕ is a spatially correlated and standard normal distributed variable generated by SOS method.

Then the initial $\phi_{qplm}^{AAOD}(t_0)$ can be calculated as

$$\phi_{qplm}^{AAOD}(t_0) = \phi_{qpl}^{AAOD}(t_0) + \frac{\pi \cdot c_{ASD} \cdot \hat{\phi}_m}{180^\circ} \quad (10)$$

where $\hat{\phi}_m$ is the offset angular and c_{ASD} is the angular spread of the AAOD of the l^{th} cluster.

The other angular parameters of the clusters, $\phi_{qpl}^{AAOA}(t)$, $\phi_{qpl}^{EAOD}(t)$, $\phi_{qpl}^{EAOA}(t)$ can be generated similarly.

Second, the delays of the NLOS components can be calculated as

$$\tau_{qp}^{lm}(t) = \tilde{\tau}_l(t) + \frac{\mathbf{D}_q^{lm}(t) + \mathbf{D}_p^{lm}(t)}{c} \quad (11)$$

where $\tilde{\tau}_l(t)$ is the virtual and unilateral exponential distributed delay between C_l^A and C_l^Z . According to the locations of the first and the last clusters, the virtual delay can be obtained as.

$$\tilde{\tau}_l(t) = -\ln \frac{1}{2} \operatorname{erfc} \left(\frac{X_l^T(\mathbf{C}_l^A(t)) + X_l^T(\mathbf{C}_l^Z(t))}{2\sqrt{\rho_\tau}(\mathbf{D}_{qp}^L(t)) + 1} \right) \quad (12)$$

where X_l^T a spatially correlated and standard normal distributed variable generated by SOS method.

Because the initial positions of the clusters cannot be determined, we use the initial positions of Tx and Rx to generate the initial virtual delay

$$\tilde{\tau}_l(t_0) = -\ln \frac{1}{2} \operatorname{erfc} \left(-\frac{X_l^T(\mathbf{A}_p^T(t_0)) + X_l^T(\mathbf{A}_q^R(t_0))}{2\sqrt{\rho_\tau}(|\mathbf{D}_{qp}^L(t_0)|) + 1} \right) \quad (13)$$

Then the initial delay of each cluster can be calculated as

$$\tau_{qp}^l(t_0) = \tilde{\tau}_l(t_0) + \tau_{qp}^L(t_0) \quad (14)$$

The initial delays of all the rays in one of the clusters are assumed to be the same. According to the initial delay and angular parameters, the initial positions of the clusters can be determined by following the method described in the QuaDRiGa model [18].

Finally, the initial power of the cluster is calculated according to the delay.

$$P_{qp}^l(t_0) = e^{-\tau_{qp}^l(t_0) \cdot g_f^{DS}(t_0)} \times 10^{-\frac{Z_n}{10}} \quad (15)$$

where Z_n represents the shadowing effect that the cluster experiences during the propagation.

Similarly, the initial power of the rays with the cluster is calculated as

$$\tilde{P}_{qp}^{lm}(t_0) = e^{-\tau_{qp}^{lm}(t_0) \cdot g_f^{DS}(t_0)} \times 10^{-\frac{Z_n}{10}} \quad (16)$$

$$P_{qp}^{lm}(t_0) = \frac{\tilde{P}_{qp}^{lm}(t_0)}{\sum_{m=1}^{M_l} \tilde{P}_{qp}^{lm}(t_0)} P_{qp}^l(t_0) \quad (17)$$

C. Update the parameters on the time axis

Following the movements of the Tx, Rx, and clusters, the positions should be updated as

$$\mathbf{A}_p^T(t) = \mathbf{A}_p^T(t_0) + \int_{t_0}^t \mathbf{v}^T(s) ds \quad (18)$$

$$\mathbf{A}_q^R(t) = \mathbf{A}_q^R(t_0) + \int_{t_0}^t \mathbf{v}^R(s) ds \quad (19)$$

$$\mathbf{C}_l^A(t) = \mathbf{C}_l^A(t_0) + \int_{t_0}^t \mathbf{v}^A(s) ds \quad (20)$$

$$\mathbf{C}_l^Z(t) = \mathbf{C}_l^Z(t_0) + \int_{t_0}^t \mathbf{v}^Z(s) ds \quad (21)$$

Then these updated positions should be substituted into (12) to calculate the delays of each ray in the clusters again.

Next, according to the updated positions of Tx, Rx, and clusters, the AAO and EAO of each ray in the clusters can be calculated as

$$\phi_{qplm}^{AAOD}(t) = \arctan\left(\frac{\mathbf{D}_p^{lm}(t)|_y}{\mathbf{D}_p^{lm}(t)|_x}\right) \quad (22)$$

$$\phi_{qplm}^{EAO}(t) = \arcsin\left(\frac{\mathbf{D}_p^{lm}(t)|_z}{|\mathbf{D}_p^{lm}(t)|}\right) \quad (23)$$

where $\mathbf{D}_p^{lm}(t)|_s$ ($s = x, y, z$) are the coordinates of x-axis, y-axis and z-axis, respectively.

The AAO and EAO can be updated similarly.

Finally, the power of the rays within the clusters is updated as (15)-(17).

D. Model the spatial and time-domain non-stationarity

The spatial and time-domain non-stationarity is modeled by describing the birth and death of the clusters under the industrial environments.

The survival probability of a cluster for the different antennas at the Tx side can be expressed as

$$P_{sur}(p, p') = e^{-\frac{\lambda_R |\mathbf{A}_p^T(t) - \mathbf{A}_{p'}^T(t)|}{D_c^a}} \quad (24)$$

$$E[N_{ng}(p, p')] = \frac{\lambda_G}{\lambda_R} (1 - P_{sur}(p, p')) \quad (25)$$

where N_{ng} represents the number of newly generated clusters. λ_G and λ_R represent the birth and death rates of the clusters, respectively. The coefficient D_c^a describes the spatial coherence distance. The typical value of D_c^a in the industrial environments is 10m. The survival probability of the clusters at the Rx side can be obtained similarly.

Furthermore, the survival probability of a cluster at different snapshots can be expressed as

$$P_{sur}(\Delta t) = e^{-\frac{\lambda_R P_F(\Delta v^R + \Delta v^T)(\Delta t)}{D_c^a}} \quad (26)$$

$$\Delta v^R = |\mathbf{v}^R - \mathbf{v}^Z|, \quad \Delta v^T = |\mathbf{v}^T - \mathbf{v}^A| \quad (27)$$

where Δt is time difference of the two snapshots, respectively. Then the number of newly generated clusters due to the movements of the USs and clusters can be determined as similar as (25).

E. Derivation of Space-Time-Frequency Correlation Function

The space-time-frequency correlation function (STFCF) of the channel is defined as

$$R_{pp'qq'}(\Delta\xi, \Delta t, \xi, t) = E[H_{qp}^*(\xi, t) H_{q'p'}(\xi + \Delta\xi, t + \Delta t)] \quad (28)$$

Substituting (7) into (28), we can get

$$R_{pp'qq'} = \sum_{i=1}^{N_F} \sum_{j=1}^{N_F} R_{pp'qq'}^{ij} \quad (29)$$

where $R_{pp'qq'}^{ij}$ is the STFCF between the i^{th} and j^{th} bins.

According to the Fourier transform, $R_{pp'qq'}^{ij}$ can be expressed as

$$R_{pp'qq'}^{ij} = \frac{K(t)}{K(t) + 1} R_{pp'qq'}^{ij,L} + \frac{1}{K(t) + 1} R_{pp'qq'}^{ij,N} \quad (30)$$

$$R_{pp'qq'}^{ij,L} = E[h_{qp}^{L*}(t) h_{q'p'}^L(t + \Delta t) \times e^{j2\pi(\xi\tau_{qp}^L(t) - (\xi + \Delta\xi)\tau_{q'p'}^L(t + \Delta t))}] \quad (31)$$

$$R_{pp'qq'}^{ij,N} = E\left[\sum_{l=1}^{N_{qp}(t)} \sum_{m=1}^{M_l} h_{qp}^{lm*}(t) h_{q'p'}^{lm}(t + \Delta t) \times P_{sur} \times e^{j2\pi(\xi\tau_{qp}^{lm}(t) - (\xi + \Delta\xi)\tau_{q'p'}^{lm}(t + \Delta t))}\right] \quad (32)$$

Furthermore, we can get several important correlation functions of the channel by simplifying the STFCF. Let $q = q'$, $p = p'$, $\Delta\xi = 0$, the autocorrelation function (ACF) can be calculated. Set $q = q'$, $p = p'$, $\Delta t = 0$, the frequency correlation function (FCF) can be obtained. The the space cross-correlation function (CCF) at the Rx(Tx) side can be achieved when $\Delta\xi = 0$, $\Delta t = 0$ and $p = p'(q = q')$.

III. RESULTS AND ANALYSIS

In this section, the results of the proposed model are validated and analyzed. The spatial consistency of the proposed model is tested by analyzing the variations of the parameters, such as, the delays and angles, along a trajectory. Then the accuracy of the proposed model is proved by the measured results. Finally, the analytical correlation functions, i.e, ACF, FCF, CCF are validated by the simulated results.

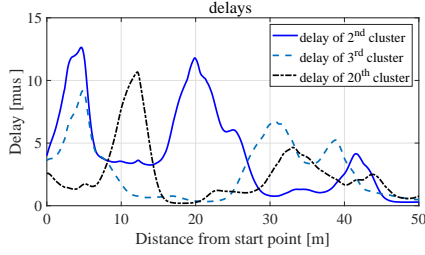


Fig. 2. The spatial consistency of the delays under the NLOS industrial environment. $f_c = 28$ GHz and $B_c = 1$ GHz. $N_B = 128$ and the position of the BS is fixed. The coordinate of the central at the BS side is [0 0 10] and the space of the adjacent antennas is two wavelengths. $N_U = 1$ and US moves along a trajectory with a length of 50m. The coordinate of the starting point is [20 30 1.5]. The number of the clusters is 20.

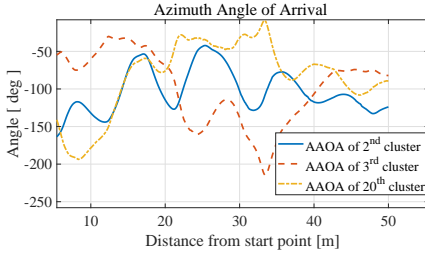


Fig. 3. The spatial consistency of the AAOAs under the NLOS industrial environment. $f_c = 28$ GHz and $B_c = 1$ GHz. $N_B = 128$ and the position of the BS is fixed. The coordinate of the central at the BS side is [0 0 10] and the space of the adjacent antennas is two wavelengths. $N_U = 1$ and US moves along a trajectory with a length of 50m. The coordinate of the starting point is [20 30 1.5]. The number of the clusters is 20.

A. spatial consistency of the proposed model

The spatial consistency of the proposed model means that the positions of the clusters should be spatially correlated. For example, two closely spaced USs should experience similar clusters. Since the positions of the clusters are determined by the parameters, such as AAOA, EAOA, AAOD, EAOD and delays, two closely spaced USs must possess similar parameters. Due to space limitations, only the simulated delays, AAOA and AAOD of several clusters when the US moves along a trajectory with a length of 50m are depicted in Fig.2-4. As seen in these figures, all the above parameters change smoothly over the trajectory, which indicates that the clusters of any two closely spaced USs are similar. Therefore, the spatial consistency is achieved in the proposed model.

B. Accuracy of the proposed model

To validate the accuracy of the proposed model, the simulated results are compared with the measured ones in [19] under two different industrial environments. The RMS delay spread is selected as the statistical parameters for the comparisons. The simulated RMS delay spread and the measured ones are shown in Fig.5. The results show that the simulated RMS delay spread match well with the measured ones, which validates the proposed model.

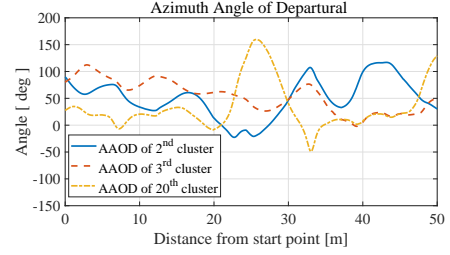


Fig. 4. The spatial consistency of the AAODs under the NLOS industrial environment. $f_c = 28$ GHz and $B_c = 1$ GHz. $N_B = 128$ and the position of the BS is fixed. The coordinate of the central at the BS side is [0 0 10] and the space of the adjacent antennas is two wavelengths. $N_U = 1$ and US moves along a trajectory with a length of 50m. The coordinate of the starting point is [20 30 1.5]. The number of the clusters is 20.

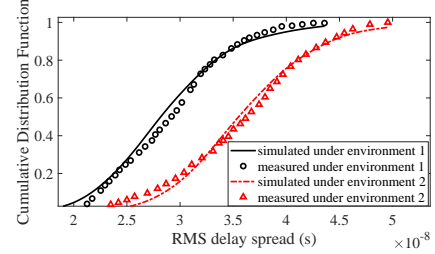


Fig. 5. The simulated and measured CDFs of RMS delay spread under two different NLOS industrial environments [19]. $f_c = 5.8$ GHz, $N_B = 1$, $N_U = 1$, $\mathbf{v}^T = 0.4$ m/s, $\mathbf{v}^R = 0$ m/s. $\lambda_G = 4$, $\lambda_R = 60$ under the environment 1 and $\lambda_G = 4$, $\lambda_R = 80$ under the environment 2.

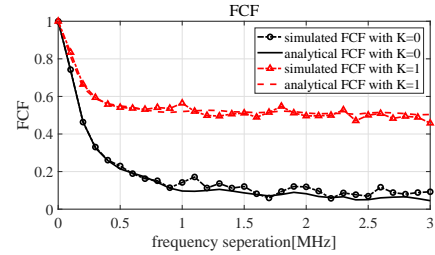


Fig. 6. The analytical FCFs compared with the simulated ones under the LOS and NLOS environments. The Rician factor is assumed to be 1 under the LOS environments. $f_c = 28$ GHz and $B_c = 1$ GHz. $N_B = 128$. The coordinate of the central at the BS side is [0 0 10] and the space of the adjacent antennas is two wavelengths. $N_U = 1$ and the coordinate is [20 30 1.5]. $\lambda_G = 80$ and $\lambda_R = 4$.

C. Accuracy of the analytical correlation functions

Finally, the analytical correlation functions of the ACF, FCF, CCF are validated by the simulated results under the LOS and NLOS environments. The Rician factor is assumed to be 1 under the LOS environments. Fig.6-8 show the analytical results compared with simulated ones. All of the correlation functions are normalized. The frequency separation, time separation and antenna index are selected as the x-ables of Fig.6-8, respectively. All the correlation functions decrease with the x-ables. All the analytical correlation functions match well with simulated ones, which proves the correctness of the analytical correlation functions.

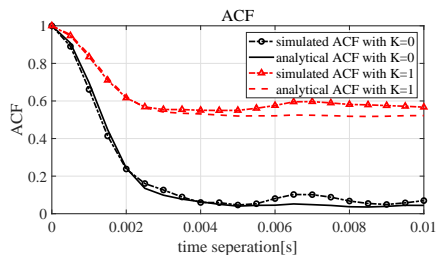


Fig. 7. The analytical ACFs compared with the simulated ones under the LOS and NLOS environments. The Rician factor is assumed to be 1 under the LOS environments. $f_c = 28$ GHz and $B_c = 1$ GHz. $N_B = 128$. The coordinate of the central at the BS side is $[0 \ 0 \ 10]$ and the space of the adjacent antennas is two wavelengths. $N_U = 1$ and the coordinate is $[20 \ 30 \ 1.5]$. $\lambda_G = 80$ and $\lambda_R = 4$. $\mathbf{v}^A = 1$ m/s and $\mathbf{v}^Z = 1$ m/s. The coefficient D_c^a is 10m.

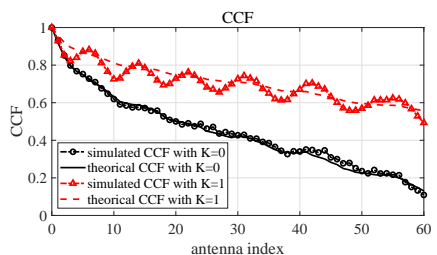


Fig. 8. The analytical CCFs compared with the simulated ones under the LOS and NLOS environments. The Rician factor is assumed to be 1 under the LOS environments. $f_c = 28$ GHz and $B_c = 1$ GHz. $N_B = 128$. The coordinate of the central at the BS side is $[0 \ 0 \ 10]$ and the space of the adjacent antennas is two wavelengths. $N_U = 1$ and the coordinate is $[20 \ 30 \ 1.5]$. $\lambda_G = 80$ and $\lambda_R = 4$. The coefficient D_c^a is 10m.

IV. CONCLUSION

In this paper, a general 3D GBSM has been proposed for the industrial IoT environments. Under the proposed framework, the power, delay, AAOA, AAOD, EAOA, and EAOD have been combined to model the CIR. The spatial consistency has been obtained by the SOS method. The spatial non-stationarity has been modeled by describing the birth and death of the clusters under the industrial environments. To support the broadband channel, the CIR has been modeled at each bin and the frequency correlation has been taken into account. Based on the proposed model, the STFCF has been derived.

Extensive simulated and measured results have been utilized to validate the accuracy proposed model. First, the delay, AAOA and AAOD have changed smoothly over the trajectory, which proves the spatial consistency of the proposed model. Then the simulated RMS delay spread has compared with the measured ones and results have shown the accuracy of the proposed model. Finally, the analytical ACF, FCF, CCF have been obtained by simplifying the STFCF and compared with the simulated ones. Results have indicated the correctness of the derived STFCF.

The proposed model may be used to design the uRLLC systems under the industrial IoT environments.

ACKNOWLEDGMENT

This work was supported by the National Natural Science Foundation of China under Grant 61801193 and 61801238, in part by the 111 Project under Grant B12018, in part by the Open Foundation of State Key Laboratory of Millimeter Waves under Grant K201918, in part by open fundation of Key Laboratory of Wireless Sensor Network and Communication, Shanghai Institute of Microsystem and Information Technology, Chinese Academy of Sciences, under Grant 20190917 and in part by the Six talent peaks project in Jiangsu Province.

REFERENCES

- [1] P. Yegani, "probability density of the power spectrum transfer function for a two-path and three-path factory radio channel," *IEEE Veh. Technol. Conf.*, pp. 477-481, May.1991.
- [2] T. S. Rappaport, S. Y. Seidel, K. Takamizawa, "Statistical channel impulse response Models for factory and open plan building radio communicate system design," *IEEE Trans. Commun.*, vol. 39, no. 5, pp. 794-807, May 1991.
- [3] P. Yegani and C. D. McGillem, "A statistical model for the factory radio channel," *IEEE Trans. Commun.*, vol.39, no.10, pp. 1445-1454, Oct. 1991.
- [4] J. Karedal, S. Wyne, P. Almers, et al. "Statistical analysis of the UWB channel in an industrial environment," *IEEE Veh. Technol. Conf.*, pp. 81-85, 2004.
- [5] C. Oestges, D. V. Janvier, and B. Clerckx, "Channel characterization of indoor wireless personal area networks," *IEEE Trans. Antennas Propaga.*, vol. 54, no. 11, pp. 3143-3150, 2006.
- [6] A. F. Molisch, D. Cassioli, C. C. Chong, "A comprehensive standardized model for ultrawideband propagation channels," *IEEE Trans. Antennas Propaga.*, vol. 54, no. 11, pp. 3151-3166, 2006.
- [7] J. Karedal, S. Wyne, P. Almers, et al, "A measurement-based statistical model for industrial ultra-wideband channels," *IEEE Trans. Wireless Commun.*, vol. 4, no. 3, pp. 3028-3037, 2005.
- [8] E. Tanghe, W. Joseph, L. Verloock, et al, "The industrial indoor channel: large-scale and temporal fading at 900, 2400, and 5200 MHz," *IEEE Trans. Wireless Commun.*, vol. 7, no. 7, pp. 2740-2751, 2008.
- [9] P. Agrawal, A. Ahlen, T. Olofsson, et al, "Long term channel characterization for energy efficient transmission in industrial environments," *IEEE Trans. Commun.* vol. 62, no. 8, pp. 3004-3014, Aug.2014.
- [10] T. Olofsson, A. Ahln, and M. Gidlund, "Modeling of the fading statistics of wireless sensor network channels in industrial environments," *IEEE Trans. Signal Process.*, vol. 64, no. 12, pp. 3021-3034.
- [11] M. Eriksson and T. Olofsson, "On long-term statistical dependences in channel gains for fixed wireless links in factories," *IEEE Trans. Commun.*, vol. 64, no. 7, pp. 3078-3091, 2016.
- [12] A. F. Molisch, D. Cassioli, C. C. Chong, "A comprehensive standardized model for ultrawideband propagation channels," *IEEE Trans. Antennas Propaga.*, vol. 54, no. 11, pp. 3151-3166, 2006.
- [13] M. Cheffena, "Industrial wireless sensor networks: channel modeling and performance evaluation," *EURASIP J. Wireless Commun. and Networking*, vol. 2012, no. 297, 2012
- [14] M. A. Matin, K. A. Yasmeeen, M. A. M. Ali, "Statistical model for UWB channel in an industrial environment," *Proc. International Conf. Microw. and millimeter wave Technol.*, pp. 1015-1017, 2018.
- [15] C.-X. Wang, S. Wu, L. Bai, et al, "Recent advances and future challenges for massive MIMO channel measurements and models," *Sci. China Inf. Sci.*, Invited paper, vol. 59, no. 2, pp. 1-16, Feb. 2016.
- [16] S. Wu, C.-X. Wang, H. M. Aggoune, et al, "A general 3-D non-stationary 5G wireless channel model," *IEEE Trans. Commun.*, vol. 66, no. 7, pp. 3065-3078, 2018.
- [17] 3GPP TR 38.901, V14.0.0, "Study on channel model for frequencies from 0.5 to 100GHz (Release 14)," Mar. 2017.
- [18] S. Jaeckel, L. Raschkowski, K. Borner, et al, "QuaDRiGa-quasi deterministic radio channel generator, user manual and documentation," Fraunhofer Heinrich Hertz institute, Tech. Rep. v2.0.0, Aug. 2017.
- [19] B. Hoffeld, D. Wieruch, L. Raschkowski, et al, "Radio channel characterization at 5.85 GHz for wireless M2M communication of industrial robots," *IEEE Wireless Commun. Networking Conf.*, 2016.